

# Resolving Ambiguity of the Kondo Temperature Determination in Mechanically Tunable Single-Molecule Kondo Systems

Martin Žonda,<sup>\*,†,‡</sup> Oleksandr Stetsovych,<sup>¶</sup> Richard Korytár,<sup>†</sup> Markus Ternes,<sup>§,||</sup>  
 Ruslan Temirov,<sup>||,⊥</sup> Andrea Raccanelli,<sup>#</sup> F. Stefan Tautz,<sup>@,△,▽</sup> Pavel Jelínek,<sup>¶,††</sup>  
 Tomáš Novotný,<sup>†</sup> and Martin Švec<sup>\*,¶,††</sup>

<sup>†</sup>*Department of Condensed Matter Physics, Faculty of Mathematics and Physics, Charles University, Ke Karlovu 5, CZ-121 16 Praha 2, Czech Republic*

<sup>‡</sup>*Institute of Physics, Albert Ludwig University of Freiburg, Hermann-Herder-Strasse 3, 79104 Freiburg, Germany*

<sup>¶</sup>*Institute of Physics, Czech Academy of Sciences, Cukrovarnická 10, CZ-162 00 Praha 6, Czech Republic*

<sup>§</sup>*Institute of Physics II B, RWTH Aachen University, 52074 Aachen, Germany*

<sup>||</sup>*Peter Grünberg Institut (PGI-3), Forschungszentrum Jülich, Germany*

<sup>⊥</sup>*University of Cologne, Faculty of Mathematics and Natural Sciences, Institute of Physics II, Germany*

<sup>#</sup>*Peter Grünberg Institute (Cryo-Lab), Forschungszentrum Jülich, Germany*

<sup>@</sup>*Peter Grünberg Institute (PGI-3), Forschungszentrum Jülich, Germany*

<sup>△</sup>*Jülich Aachen Research Alliance (JARA), Fundamentals of Future Information Technology, Germany*

<sup>▽</sup>*Institute of Physics IV A, RWTH Aachen University, Germany*

<sup>††</sup>*RCPTM, Palacky University, Šlechtitelu 27, 783 71, Olomouc, Czech Republic.*

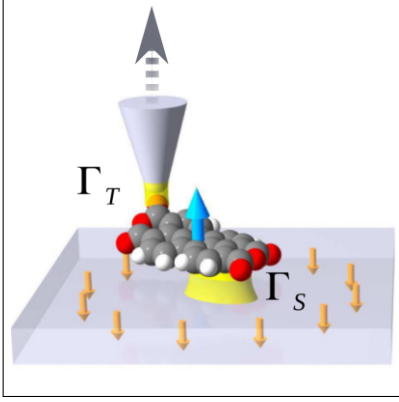
E-mail: martin.zonda@karlov.mff.cuni.cz; svec@fzu.cz

## Abstract

Determination of the molecular Kondo temperature  $T_K$  poses a challenge in most cases when the experimental temperature cannot be tuned to a sufficient extent. We show how this ambiguity can be resolved if additional control parameters are present, such as magnetic field and mechanical gating. We record the evolution of the differential conductance by lifting an individual molecule from the metal surface with the tip of a scanning tunneling microscope. By fitting the measured conductance spectra with the single impurity Anderson model we are able to demonstrate that the lifting tunes the junction continuously from the strongly correlated

Kondo-singlet to the free spin  $1/2$  ground state. In the crossover regime, where  $T_K$  is similar to the temperature of experiment, the fitting yields ambiguous estimates of  $T_K$  varying by an order of magnitude. We show that analysis of the conductance measured in two distinct external magnetic fields can be used to resolve this problem.

# Graphical TOC Entry



The Kondo effect is one of the most prominent many-particle phenomena in which a magnetic moment of an atom or molecule is screened by the itinerant electrons of the metallic substrate.<sup>1</sup> Its highly correlated singlet ground state is fully characterized by the energy  $k_B T_K$ , where  $k_B$  is the Boltzmann constant and  $T_K$  the Kondo temperature.  $T_K$  depends exponentially on the strength of the antiferromagnetic exchange coupling between the localized moment and the metallic substrate. The Kondo effect is fundamental to various phenomena at nanoscale, ranging from the occurrence of zero-bias anomalies in transport measurements through quantum dots,<sup>2–4</sup> nanowires,<sup>5</sup> single atoms and molecular junctions,<sup>6</sup> and molecular magnets,<sup>7–11</sup> to quantum critical phenomena,<sup>12–14</sup> and has implications for spintronics.<sup>15</sup>

Scanning probe microscopy (SPM) allows studies of the Kondo effect in atomic and molecular systems with unprecedented detail. Since the first SPM observations of the Kondo effect on individual magnetic adatoms adsorbed on noble metal surfaces<sup>7,16–18</sup> it has become usual to extract  $T_K$  from the differential  $dI/dV(V)$  conductance spectra measured over the Kondo impurity: When the experimental temperature  $T_{\text{exp}}$  is much lower than  $T_K$  ( $T_{\text{exp}} \ll T_K$ ), the system is in the strongly-correlated Kondo singlet state. The spectra are dominated by a zero-bias Kondo resonance whose half width at half maximum (HWHM) is directly proportional to  $k_B T_K$ .<sup>1</sup> However, when  $T_{\text{exp}} \gg T_K$ , the spin of the magnetic impurity becomes asymptotically free and the tunneling spectra are best described by a perturbative spin-flip model, yielding temperature-broadened logarithmic singularities at zero bias.<sup>19–21</sup>

The crossover between both regimes can be controlled via substrate hybridization.<sup>22–26</sup> However, in spite of a significant experimental effort,<sup>3,4,22–26</sup> a comprehensive study of the continuous evolution of  $T_K$  still poses a significant challenge. One of the reasons is the difficulty in determining the relevant energy scale in the crossover regime from experimental data, which can lead to a drastically incorrect estimate of  $T_K$ .<sup>20,27</sup> In this Letter we provide both the experimental data and the recipe for their quan-

titative analysis which are together showing a continuous evolution from strongly correlated Kondo-regime to the free spin 1/2 ground-state. Our key finding is that  $T_K$  cannot be deduced unambiguously from the *experimental*  $dI/dV$  spectra unless additional information is taken into account. We show that incipient (not fully evolved) Zeeman splitting is sufficient for this goal if two cases with distinct magnetic fields are analyzed together.

We use the archetypical 3,4,9,10-perylene-tetracarboxylic-dianhydride (PTCDA) molecule on the Ag(111) surface as our model system. The tuning of the hybridization is achieved by lifting the molecule with the tip of an SPM from the surface.<sup>22–25</sup> The variation of the tip-sample distance during the lifting process provides effective control over the (dominant) coupling  $\Gamma_S$  between the singly occupied molecular orbital and the substrate. It is thus possible to transform the system from the strongly correlated Kondo singlet to the free spin 1/2 ground state (Fig. 1).

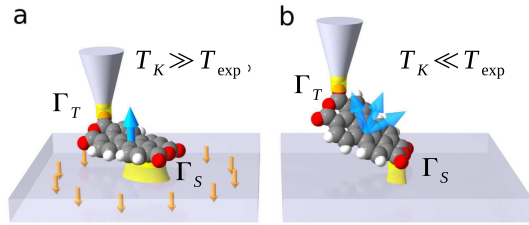


Figure 1: Schematics of the experiment. Lifting the molecule by changing the tip-sample distance  $z$  controls the coupling  $\Gamma_S$  between the molecule and the substrate, and consequently, the system transforms from the strong coupling regime with  $T_K \gg T_{\text{exp}}$  (a), to the weakly-coupled spin-flip regime with  $T_K \ll T_{\text{exp}}$  (b). The coupling  $\Gamma_T$  of the molecule to the tip remains small and mainly constant.

In the lifting experiments, we record  $dI/dV$  spectra as a function of the vertical tip position  $z$ , where  $z = 0$  is defined as the tip position at which the tip apex atom makes contact with one of the carboxylic oxygen atoms of PTCDA (Fig. 1). This corresponds to a tip-sample distance of approximately 6.3 Å.<sup>23</sup> All experiments in this study are carried out at a

base temperature of 1.2 K. We focus on tip positions  $z \gtrsim 200$  pm, where a symmetric resonance at zero bias is observed in the  $dI/dV$  spectra.

The evolution of the  $dI/dV$  spectra in the range  $z < 200$  pm was previously discussed in Refs.<sup>22–25</sup> In the flat adsorbed geometry ( $z \ll 200$  pm) the occupancy of the lowest unoccupied molecular orbital (LUMO) is close to 2 electrons. Reducing the occupancy of the LUMO to 1 by lifting the molecule leads to the Kondo effect regime that we analyze here in detail. Fig. 2a displays five subsequently acquired spectra at  $B = 0$ . The broad Kondo peak at  $z = 250$  pm becomes progressively sharper as the molecule is decoupled from the substrate by increasing  $z$ , and the overall conductance is gradually decreasing.

As the first step to rationalize the data in Fig. 2a, we fit the spectra with the standard phenomenological Frota formula (blue curves in Fig. 2a),<sup>29</sup>

$$\frac{dI}{dV}(V) \propto \mathcal{R} \sqrt{\frac{i\Gamma_F}{i\Gamma_F + eV}}, \quad (1)$$

where the Frota width  $\Gamma_F$  is related to the Kondo temperature by  $k_B T_K = 0.686 \Gamma_F$  which holds when  $T_K \gg T_{\text{exp}}$ <sup>a</sup>. We observe a drop in the apparent  $T_K$  from  $\approx 32$  K at  $z \simeq 200$  pm to  $\approx 4$  K at  $z \simeq 350$  pm (Fig. 2b)<sup>b</sup>. However, the apparent  $T_K$  steadily rises when  $z$  is increased further. The observed minimum is highly suspicious because  $T_K$  depends exponentially on the total coupling ( $\Gamma = \Gamma_T + \Gamma_S$ ) of the molecule to tip ( $\Gamma_T$ ) and sample ( $\Gamma_S$ ). Specifically,  $T_K$  calculated for the suitable spin 1/2 single impurity Anderson model (SIAM) reads<sup>30,31</sup>

$$k_B T_K = 0.29 \sqrt{\Gamma U} \exp\left(-\frac{\pi U}{8\Gamma}\right), \quad (2)$$

<sup>a</sup>The value of the numerical prefactor depends on the definition of  $T_K$ . We use the Wilson's definition (for wide band limit) as it is common in NRG, perturbation theory, and Bethe Ansatz studies. A short discussion on how this definition relates to other commonly used ones can be found in Ref.<sup>28</sup>

<sup>b</sup>Note that a simple finite-temperature correction (Ref.,<sup>20</sup> Suppl. Note 2) does not differ significantly from the zero-temperature results.

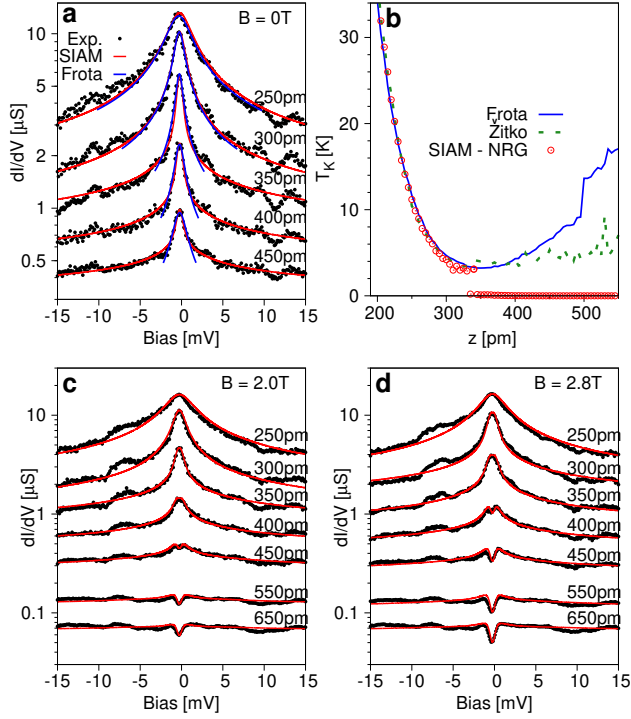


Figure 2: (a) Spectra obtained for  $B = 0$  at different tip heights  $z$  (dots) and their fits using Eq. (1) (blue lines) and NRG calculations (red lines). (b) Apparent  $T_K$  extracted from the line shapes using different types of fits: Frota fit (full line), procedure introduced by Žitko<sup>28</sup> (dashed line) and direct fit to SIAM using NRG, for a broad range of the tip-substrate distances  $z$ . (c, d)  $dI/dV$  spectra (dots) for  $B = 2.0$  (c) and  $2.8$  T (d) and NRG-based fits (lines). Note the logarithmic scale on the vertical axis in panels (a), (c), and (d).

where  $U$  is the intraorbital Coulomb repulsion<sup>30,31</sup> and the particle-hole symmetry is assumed. Because it is expected that lifting reduces  $\Gamma_S$  but keeps  $\Gamma_T$  approximately constant, any rise of  $T_K$  with increasing  $z$  is counterintuitive. The first hint, that the problem might be in the estimation of  $T_K$  comes from an alternative fitting procedure proposed by Žitko.<sup>28</sup> Although it leads to a similar behavior as Frota fitting (Fig. 2b) the increase of  $T_K$  is much less dramatic.

Recalling that the Frota fit is bound to fail if  $T_K \lesssim T_{\text{exp}}$  we turn to the numerical renormalization group (NRG) theory. Because the contact of the PTCDA molecule to the tip is electronically weak,<sup>32</sup> we can assume a strongly

asymmetric junction, resulting in an asymmetry parameter  $a \equiv \Gamma_T/\Gamma_S \ll 1$  (Fig. 1). This justifies the interpretation of the  $dI/dV$  spectra as temperature-broadened equilibrium Kondo spectral functions, calculated as<sup>33</sup>

$$\frac{dI}{dV}(V) = -G \int_{-\infty}^{\infty} d\omega \pi \Gamma \rho(\omega, \Gamma, T, B) f'(\omega - eV, T), \quad (3)$$

where the impurity spectral function  $\rho(\omega, \Gamma, T, B)$  of the SIAM calculated with NRG depends on the temperature  $T$ , magnetic field  $B$ , and total coupling  $\Gamma$ . Here,  $f'(\omega, T)$  is the derivative of the Fermi-Dirac distribution with respect to  $\omega$ .  $\Gamma_T$  and  $\Gamma_S$  are assumed to be independent of  $\omega$  and  $B$ . Hence,

$$G \equiv \frac{2e^2}{h} \frac{4\Gamma_S\Gamma_T}{\Gamma^2} = \frac{2e^2}{h} \frac{4a}{(1+a)^2} \quad (4)$$

depends only on the coupling asymmetry  $a$ , while the integrand in Eq. (3) depends on the total coupling  $\Gamma$ .

The SIAM spectral functions calculated with NRG are commonly used for a qualitative comparison with experiments.<sup>34</sup> However, a direct least-squares fitting of experimental spectra (shown, e.g., in Fig. 2a,c,d) is largely avoided because of its computational complexity (for recent counterexamples see, e.g., Refs.<sup>35–37</sup>). Nevertheless, as we discuss in detail in the Supporting Information (SI), modern NRG packages<sup>38</sup> make this task manageable. In our calculations we fix  $T$  and  $B$ , and we have also found out that varying  $U$  within the expected range of  $0.5 - 1$  eV does not significantly change the fitted  $T_K$  as its influence can be mitigated by varying  $\Gamma$ . Therefore, our relevant fitting parameters are  $G$  and  $\Gamma/U$  (see Eq. (2)). In practice we precalculated large sets of spectral functions of SIAM for a dense mesh of  $\Gamma/U$  values with  $G = 1$ . These are then used to approximate the experimental  $dI/dV$  curves by first fitting the optimal  $G$  and then picking  $\Gamma/U$  curves with the minimal sum of the least-squares residuals.

Kondo temperature obtained from the NRG fits (Fig. 2b) initially follows the Frota-estimated  $T_K$ . However, around its minimum value at  $z \approx 350$  pm, the NRG fit drops below

1K. This is in compliance with the expectation that  $T_K$  should monotonously decrease with increasing  $z$ . Nonetheless, one still has to be cautious with the interpretation of the results. Especially intriguing is the sudden discontinuous drop of  $T_K$  over more than an order of magnitude. In addition, it is important to note that an analogous study of the weak coupling regime in a different system and with a different fitting procedure showed that the determination of  $T_K$  from just the zero-field data can be tricky and even erroneous.<sup>20</sup>

Therefore, in order to investigate the peculiar behavior of  $T_K$  with changing  $z$  and to stabilize the fitting in the (expected) weak coupling regime we repeated the lifting experiments in finite magnetic fields (Fig. 2c,d and Fig. 3a,b).

The presence of the magnetic field leads to a splitting of the zero-bias conductance peak at sufficiently large  $z$ . After an initial increase, the splitting remains constant during further tip retraction, as seen in Fig. 3a,b.

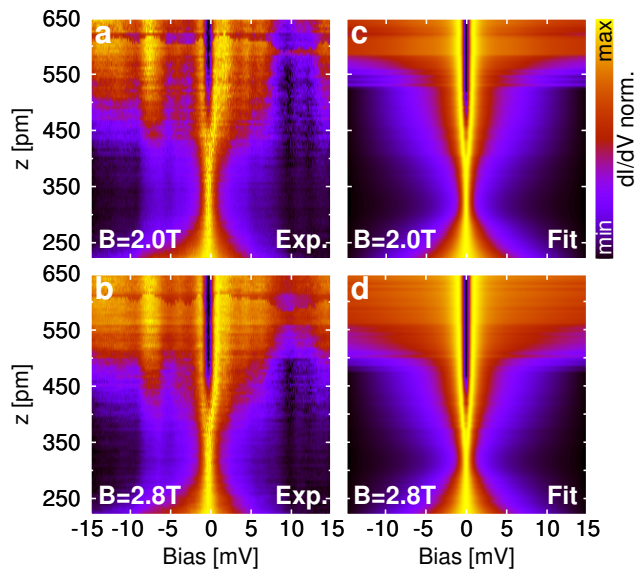


Figure 3: (a, b) Experimental data represented by spectral intensity maps. Each measured spectrum (horizontal line) is normalized by subtracting its minimum value and dividing by its total range. (c, d) Equivalent maps obtained from the modeled spectra using NRG.

For a visible splitting of the Kondo resonance, the Zeeman energy of  $g\mu_B B \gtrsim 2k_B T_K$  is needed.<sup>39,40</sup> The fact that the splitting occurs at  $z \simeq 450$  pm for  $B = 2.0$  T but al-

ready at  $z \simeq 400$  pm for 2.8 T implies that  $T_K(z = 450 \text{ pm}) < T_K(z = 400 \text{ pm})$ . This is in a direct contradiction with the picture of a constant or even increasing  $T_K$  for  $z > 350$  pm as drawn from a simple Frota fit in Fig. 2b.

The NRG fits account for both, the changing width of the Kondo resonance, as well as its splitting for  $g\mu_B B \gtrsim 2k_B T_K$  (Fig. 3)<sup>c</sup>. From the NRG fits, two important results are principally available: a mapping  $z \rightarrow \Gamma/U$ , and, via Eq. (2), the Kondo temperature as a function of the tip height  $T_K(z)$ .

The function  $T_K(z)$  obtained from the NRG-based fitting for various  $B$  drops roughly exponentially by nine orders of magnitude over the experimental  $z$  range (Fig. 4a). Clearly, the huge discrepancy between the Frota fit and the NRG-based fit for  $z \gtrsim 350$  pm is a direct consequence of the fact that in the weak-coupling regime the  $B = 0$  zero-bias anomaly is not a Kondo resonance but a temperature-broadened logarithmic singularity, whose shape nevertheless resembles the Frota function. Consequently, the application of Eq. (1) leads to a dramatic overestimation of  $T_K$  by several orders of magnitude (Fig. 4a). In contrast, the split Kondo peak at sufficiently high  $B$  makes the data sets in this  $z$  range feature-rich, which allows a meaningful fit with NRG-based SIAM spectra.

However, the direct NRG fits at finite  $B$  do not solve the mystery of the discontinuous drop of the  $T_K$  in the intermediate coupling regime, as they show the same feature. Nevertheless, the fact that the drop happens at different  $z$  for different fields  $B$  and even shows some instabilities does not point to a true physical interpretation but rather again to a problem with the fitting procedure.

Indeed, while the NRG-based fitting works well for the strong coupling as well as for the split resonance in the weak-coupling limit, it is problematic in the crossover regime where  $T_K \simeq T_{\text{exp}}$  (shaded blue area in Fig. 4). The reason is that the width of the yet unsplit Kondo peak in this regime is not very sensitive to  $T_K$

<sup>c</sup>The experimental  $dI/dV$  displays additional features that we interpret as arising from inelastic tunneling processes, see SI for details.



(or,  $\Gamma/U$ ). This produces fitting instabilities because the change of the height of the peak, which *is* sensitive to  $\Gamma/U$ , can be mimicked by the variation of the other fitting parameter  $G$ . This is demonstrated in the inset of Fig. 4a where by tuning  $G$  a very good fit of the experimental data from the problematic regime can be achieved by significantly different values of  $\Gamma/U$ . As a consequence, no unique mapping  $z \rightarrow \Gamma/U$  can be established in this range by directly comparing experimental and theoretical spectra unless the prefactor  $G$  is eliminated from the fitting.

We have found out that a convenient way to surmount this difficulty is to assume that  $G$  does not depend on  $B$  in the crossover regime and investigate the  $G$  independent ratio  $\gamma(B_1, B_2) = [dI/dV(0, B_1)]/[dI/dV(0, B_2)]$  between zero-bias conductances obtained at two significantly different magnetic field strengths  $B_x$ . In particular one with  $g\mu_B B > 2k_B T_{\text{exp}}$ , and the other with  $g\mu_B B < 2k_B T_{\text{exp}}$ , e.g., at  $B = 2.8$  T and 1 T as plotted in Fig. 4b.

For small  $z$ , we find  $\gamma \approx 1$ , because here  $T_K > T_{\text{exp}}$  and both magnetic fields are too small to affect the Kondo resonance. For large  $z$ , we find  $\gamma < 1$ , because the  $B$ -field of 2.8 T splits the Kondo resonance, leading to a reduced zero-bias conductance. In the crossover regime  $\gamma$  changes rapidly and nonlinearly (blue shaded area in Fig. 4b where circles represent experimental data). Yet, there is no sign of a discontinuity in the experimental data. Aligning this rapidly changing curve with the same quantity calculated for SIAM by NRG as a function of  $\Gamma/U$  (for details see SI) allows us to establish an unambiguous mapping  $z \rightarrow \Gamma/U$  in the crossover regime (Fig. 4b). Given this, the correct smooth behavior of  $T_K(z)$  can be determined by Eq. (2) (full red circles in Fig. 4a).

Because the corrected  $T_K$  in the crossover regime is estimated using only zero-bias conductance we also provide a consistency test of  $z \rightarrow \Gamma/U$  mapping. We refit the complete  $dI/dV$  evolution using  $G$  as the only remaining free parameter in the crossover regime [Fig. 3(c,d)]. We demonstrate the quality of the fit by comparing the HWHM of the experimental and NRG-calculated spectra in Fig. 4c.

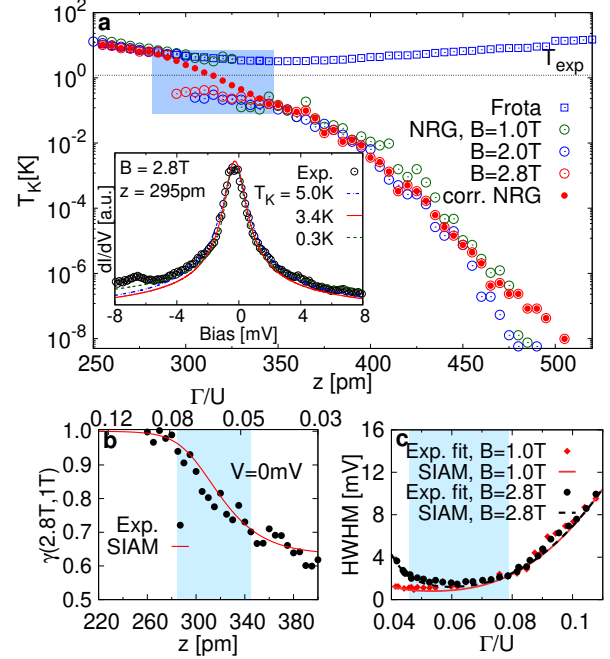


Figure 4: (a) Kondo temperature  $T_K$  as determined by Frota approximation (blue squares) for  $B = 0$ , direct NRG-based SIAM fitting (empty circles) for  $B \neq 0$  and corrected NRG fitting discussed in the text. The inset demonstrates that experimental  $dI/dV$  can be in the crossover region (blue rectangle) fitted with different values of  $\Gamma/U$  (0.051, 0.070, 0.075) leading to huge uncertainty in the estimation of  $T_K$ . (b) Ratio  $\gamma(B_1, B_2)$  at  $B_1 = 2.8$  T and  $B_2 = 1$  T (dots: experimental data, line: NRG fit). The ratio changes strongly in the transition regime (blue-shaded area) enabling the determination of  $\Gamma/U$ . The upper x-scale shows some values of  $\Gamma/U$  at respective  $z$ . (c) The HWHM of the  $B = 1$  T and 2.8 T data sets are almost constant in the transition regime (blue-shaded area), illustrating the fitting complication.

The agreement between experiment and theory is excellent throughout the crossover regime where we observe a very weak dependence of the HWHM on  $\Gamma/U$ . It is this weak dependence of HWHM on  $\Gamma/U$  that produced an ambiguity in our initial attempt to achieve  $z \rightarrow \Gamma/U$  mapping by comparing experimental and NRG-based conductance spectra. Outside the crossover regime, the HWHM rapidly rises, either because of an increasing  $T_K$  (right) or the incipient split of the Kondo resonance by the applied magnetic field (left).

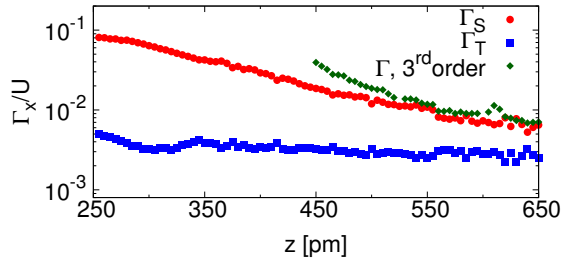


Figure 5: Extracted coupling strengths of the molecule to the substrate  $\Gamma_S/U$  and tip  $\Gamma_T/U$ , respectively, and using the third order perturbation theory showing the total  $\Gamma/U$ .<sup>21</sup>

An additional benefit of the above consistency test is the reliable extraction of  $G$  in the otherwise problematic crossover regime. Consequently, we can use Eq. (4) together with  $\Gamma = \Gamma_S + \Gamma_T$  to determine the coupling constants  $\Gamma_T/U$  and  $\Gamma_S/U$  separately (Fig. 5). We find that across the complete  $z$  range studied here,  $\Gamma_S \gg \Gamma_T$ . This retroactively justifies the model underlying Eq. (3), that is, the approximation of the molecule being equilibrated with the substrate and the tip serving as a weak probe of the spectral function. Moreover, while  $\Gamma_T/U$  varies only little,  $\Gamma_S/U$  decreases from 0.1 at  $z = 250$  pm to 0.007 at  $z = 630$  pm. This is a direct consequence of the dehybridization upon lifting the molecule. We note that the  $\Gamma_S/U$  found here are in agreement with values independently calculated with *ab initio* methods.<sup>23,25</sup> In addition, in the weak-coupling regime (the inelastic spin-flip) third-order perturbation theory<sup>19,21</sup> yields similar estimates of the overall  $\Gamma/U$  (dominated by  $\Gamma_S/U$ ), as Fig. 5 shows.

In summary, we have shown that lifting a spin-1/2 molecule from the metal surface allowed us to tune the system continuously from the strongly coupled Kondo regime to weakly coupled spin-flip regime. The detailed analysis of experimental data revealed inherent difficulties to reliably obtain  $T_K$  when thermal and Kondo energy scales are similar. However, we show that this problem can be tackled if additional data measured in magnetic fields, when the Zeeman energy is larger than the thermal energy, is used, even when the splitting of the zero bias anomaly is not present yet. Furthermore, our scheme allows us to separate the coupling strengths to the two electron leads in asymmetrically coupled Kondo systems.

Note that Kondo temperature is the principal property of adsorbed open-shell molecules in which Kondo screening is active. Its value determines the resulting functionality of the open-shell adsorbate. For instance, if the molecular magnetic moment needs to be stabilized, the respective  $T_K$  must be decreased below  $T_{\text{exp}}$ . On the other hand, if spin degeneracy is not wanted,  $T_K$  must be increased. Therefore, the unambiguous determination of  $T_K$  paves the way to achieving control over spin degrees of freedom at the nanoscale.

**Acknowledgement** T. N. and M. Ž. acknowledge support by the Czech Science Foundation via Project No. 16-19640S and M. S. via No. 17-24210Y, P. J. was supported by Praemium Academie of the Czech Academy of Sciences and GACR 20-13692X. We acknowledge CzechNanoLab Research Infrastructure supported by MEYS CR (LM2018110). M. T. was supported by the Heisenberg Program (Grant No. TE 833/2-1) of the Deutsche Forschungsgemeinschaft, and R. K. from the PRIMUS/Sci/09 programme of the Charles University. R.T. acknowledges support from the Young Investigator Group program (Grant No. VH-NG-514) of the Helmholtz Association. The authors thank M. Thoss, B. Lechtenberg, F. B. Anders and D. M. Fugger for helpful discussions.

Supporting Information: details on the sample preparation, theoretical model, the fitting

procedures and analysis of additional features of the experimental  $dI/dV$ . SI also includes additional Refs.<sup>41–50</sup>

## References

- (1) Hewson, A. C. *Kondo Problem to Heavy Fermions, The*; Cambridge University Press: Cambridge, 1997.
- (2) Goldhaber-Gordon, D.; Shtrikman, H.; Mahalu, D.; Abusch-Magder, D.; Meirav, U.; Kastner, M. A. Kondo Effect in a Single-Electron Transistor. *Nature* **1998**, *391*, 156.
- (3) Parks, J. J.; Champagne, A. R.; Hutchison, G. R.; Flores-Torres, S.; Abruña, H. D.; Ralph, D. C. Tuning the Kondo Effect with a Mechanically Controllable Break Junction. *Phys. Rev. Lett.* **2007**, *99*, 026601.
- (4) Parks, J. J.; Champagne, A. R.; Costi, T. A.; Shum, W. W.; Pasupathy, A. N.; Neuscamman, E.; Flores-Torres, S.; Cornaglia, P. S.; Aligia, A. A.; Balseiro, C. A. et al. Mechanical Control of Spin States in Spin-1 Molecules and the Underscreened Kondo Effect. *Science* **2010**, *328*, 1370.
- (5) Nygård, J.; Cobden, D. H.; Lindelof, P. E. Kondo Physics in Carbon Nanotubes. *Nature* **2000**, *408*, 342.
- (6) Evers, F.; Korytár, R.; Tewari, S.; van Ruitenbeek, J. M. Advances and challenges in single-molecule electron transport. *Reviews of Modern Physics* **2020**, *92*, 035001.
- (7) Madhavan, V.; Chen, W.; Jamneala, T.; Crommie, M. F.; Wingreen, N. S. Tunneling into a Single Magnetic Atom: Spectroscopic Evidence of the Kondo Resonance. *Science* **1998**, *280*, 567.
- (8) Yu, L. H.; Natelson, D. The Kondo Effect in  $C_{60}$  Single-Molecule Transistors. *Nano Lett.* **2004**, *4*, 79.
- (9) Otte, A. F.; Ternes, M.; Loth, S.; von Bergmann, K.; Brune, H.; Lutz, C. P.; Hirjibehedin, C. F.; Heinrich, A. J. The Role of Magnetic Anisotropy in the Kondo Effect. *Nature Physics* **2008**, *4*, 847.
- (10) Coronado, E. Molecular magnetism: from chemical design to spin control in molecules, materials and devices. *Nature Reviews Materials* **2020**, *5*, 87–104.
- (11) Chen, H.; Frauhammer, T.; Sasaki, S.; Yamada, T. K.; Wulfhekel, W. Interplay between point symmetry, oxidation state, and the Kondo effect in 3d transition metal acetylacetonate molecules on Cu(111). *Phys. Rev. B* **2021**, *103*, 085423.
- (12) (a) Jones, B. A.; Varma, C. M.; Wilkens, J. W. Low-temperature properties of the two-impurity Kondo Hamiltonian. *Phys. Rev. B* **1988**, *61*, 125; (b) Jones, B. A.; Varma, C. M. Critical point in the solution of the two magnetic impurity problem. *Phys. Rev. B* **1989**, *40*, 324.
- (13) Lechtenberg, B.; Eickhoff, F.; Anders, F. B. Realistic quantum critical point in one-dimensional two-impurity models. *Phys. Rev. B* **2017**, *96*, 041109.
- (14) Esat, T.; Lechtenberg, B.; Deilmann, T.; Wagner, C.; Krüger, P.; Temirov, R.; Rohlfing, M.; Anders, F. B.; Tautz, F. S. A chemically driven quantum phase transition in a two-molecule Kondo system. *Nature Physics* **2016**, *12*, 867.
- (15) von Bergmann, K.; Ternes, M.; Loth, S.; Lutz, C. P.; Heinrich, A. J. Spin-Polarization of the Split Kondo State. *Phys. Rev. Lett.* **2015**, *114*, 076601.
- (16) Li, J. T.; Schneider, W. D.; Berndt, R.; Delley, B. Kondo Scattering Observed at a Single Magnetic Impurity. *Phys. Rev. Lett.* **1998**, *80*, 2893.
- (17) Madhavan, V.; Chen, W.; Jamneala, T.; Crommie, M. F.; Wingreen, N. S. Local spectroscopy of a Kondo impurity: Co on Au(111). *Phys. Rev. B* **2001**, *64*, 165412.



- (18) Knorr, N.; Schneider, M. A.; Diekhoner, L.; Wahl, P.; Kern, K. Kondo Effect of Single Co Adatoms on Cu Surfaces. *Phys. Rev. Lett.* **2002**, *88*, 096804.
- (19) (a) Appelbaum, J. A. “ $s - D$ ” Exchange Model of Zero-Bias Tunneling Anomalies. *Phys. Rev. Lett.* **1966**, *17*, 91; (b) Appelbaum, J. A. Exchange Model of Zero-Bias Tunneling Anomalies. *Phys. Rev.* **1967**, *154*, 633.
- (20) Zhang, Y.; Kahle, S.; Herden, T.; Stroh, C.; Mayor, M.; Schlickum, U.; Ternes, M.; Wahl, P.; Kern, K. Temperature and magnetic field dependence of a Kondo system in the weak coupling regime. *Nature Communications* **2013**, *4*, 2110.
- (21) Ternes, M. Spin Excitations and Correlations in Scanning Tunneling Spectroscopy. *New J. Phys.* **2015**, *17*, 063016.
- (22) Temirov, R.; Lassise, A.; Anders, F. B.; Tautz, F. S. Kondo effect by controlled cleavage of a single-molecule contact. *Nanotechnology* **2008**, *19*, 065401.
- (23) Greuling, A.; Rohlfing, M.; Temirov, R.; Tautz, F. S.; Anders, F. B. Ab initio study of a mechanically gated molecule: From weak to strong correlation. *Phys. Rev. B* **2011**, *84*, 125413.
- (24) Toher, C.; Temirov, R.; Greuling, A.; Pump, F.; Kaczmariski, M.; Cuniberti, G.; Rohlfing, M.; Tautz, F. S. Electrical transport through a mechanically gated molecular wire. *Phys. Rev. B* **2011**, *83*, 155402.
- (25) Greuling, A.; Temirov, R.; Lechtenberg, B.; Anders, F. B.; Rohlfing, M.; Tautz, F. S. Spectral properties of a molecular wire in the Kondo regime. *Phys. Stat. Sol. B* **2013**, *250*, 2386.
- (26) Oberg, J. C.; Calvo, M. R.; Delgado, F.; Moro-Lagares, M.; Serrate, D.; Jacob, D.; Fernández-Rossier, J.; Hirjibehedin, C. F. Control of single-spin magnetic anisotropy by exchange coupling. *Nature Nanotechnology* **2013**, *9*, 64.
- (27) Gruber, M.; Weissmann, M.; Berndt, R. The Kondo Resonance Line Shape in Scanning Tunnelling Spectroscopy: Instrumental Aspects. *J. Phys.: Condens. Matter* **2018**, *30*, 424001.
- (28) Žitko, R. Kondo resonance lineshape of magnetic adatoms on decoupling layers. *Phys. Rev. B* **2011**, *84*, 195116.
- (29) (a) Frota, H. O.; Oliveira, L. N. Photoemission spectroscopy for the spin-degenerate Anderson model. *Phys. Rev. B* **1986**, *33*, 7871; (b) Frota, H. O. Shape of the Kondo resonance. *Phys. Rev. B* **1992**, *45*, 1096.
- (30) Haldane, F. D. M. Theory of the atomic limit of the Anderson model. I. Perturbation expansions re-examined. *Journal of Physics C: Solid State Physics* **1978**, *11*, 5015.
- (31) Krishna-murthy, H. R.; Wilkins, J. W.; Wilson, K. G. Renormalization-group approach to the Anderson model of dilute magnetic alloys. I. Static properties for the symmetric case. *Phys. Rev. B* **1980**, *21*, 1003–1043.
- (32) Temirov, R.; Green, M. F. B.; Friedrich, N.; Leinen, P.; Esat, T.; Chmielniak, P.; Sarwar, S.; Rawson, J.; Kögerler, P.; Wagner, C. et al. Molecular model of a quantum dot beyond the constant interaction approximation. *Phys. Rev. Lett.* **2018**, *120*, 206801.
- (33) Esat, T.; Deilmann, T.; Lechtenberg, B.; Wagner, C.; Krüger, P.; Temirov, R.; Anders, F. B.; Rohlfing, M.; Tautz, F. S. Transferring spin into an extended  $\pi$  orbital of a large molecule. *Phys. Rev. B* **2015**, *91*, 144415.
- (34) Bulla, R.; Costi, T. A.; Pruschke, T. Numerical renormalization group method for quantum impurity systems. *Rev. Mod. Phys.* **2008**, *80*, 395–450.

- (35) Jiang, Y.; Lo, P.-W.; May, D.; Li, G.; Guo, G.-Y.; Anders, F. B.; Taniguchi, T.; Watanabe, K.; Mao, J.; Andrei, E. Y. Inducing Kondo screening of vacancy magnetic moments in graphene with gating and local curvature. *Nature Communications* **2018**, *9*, 2349.
- (36) Minamitani, E.; Fu, Y.-S.; Xue, Q.-K.; Kim, Y.; Watanabe, S. Spatially extended underscreened Kondo state from collective molecular spin. *Phys. Rev. B* **2015**, *92*, 075144.
- (37) Sturm, E. J.; Carbone, M. R.; Lu, D.; Weichselbaum, A.; Konik, R. M. Predicting impurity spectral functions using machine learning. *arXiv e-prints* **2020**, arXiv:2011.10719.
- (38) Žitko, R. NRG Ljubljana - open source numerical renormalization group code. *Zenodo* **2021**, Version 8f90ac4.
- (39) Costi, T. A. Kondo Effect in a Magnetic Field and the Magnetoresistivity of Kondo Alloys. *Phys. Rev. Lett.* **2000**, *85*, 1504.
- (40) Žitko, R. Many-particle effects in resonant tunneling of electrons through nanostructures. Ph.D. thesis, University of Ljubljana, 2007.
- (41) Schiller, A.; Hershfield, S. Theory of scanning tunneling spectroscopy of a magnetic adatom on a metallic surface. *Phys. Rev. B* **2000**, *61*, 9036–9046.
- (42) Žitko, R.; Pruschke, T. Energy resolution and discretization artifacts in the numerical renormalization group. *Phys. Rev. B* **2009**, *79*, 085106.
- (43) Weichselbaum, A.; von Delft, J. Sum-Rule Conserving Spectral Functions from the Numerical Renormalization Group. *Phys. Rev. Lett.* **2007**, *99*, 076402.
- (44) Campo, V. L.; Oliveira, L. N. Alternative discretization in the numerical renormalization-group method. *Phys. Rev. B* **2005**, *72*, 104432.
- (45) Žitko, R.; Peters, R.; Pruschke, T. Splitting of the Kondo resonance in anisotropic magnetic impurities on surfaces. *New J. Phys.* **2009**, *11*, 053003.
- (46) Wolf, E. L.; Losee, D. L.  $g$ -shifts in the "s-d" exchange theory of zero-bias tunneling anomalies. *Phys. Lett. A* **1969**, *29*, 334.
- (47) Paulsson, M.; Frederiksen, T.; Brandbyge, M. Modeling inelastic phonon scattering in atomic-and molecular-wire junctions. *Physical Review B* **2005**, *72*, 201101.
- (48) Xu, C.; Chiang, C.-l.; Han, Z.; Ho, W. Nature of Asymmetry in the Vibrational Line Shape of Single-Molecule Inelastic Electron Tunneling Spectroscopy with the STM. *Physical Review Letters* **2016**, *116*, 166101.
- (49) Paulsson, M.; Frederiksen, T.; Brandbyge, M. Phonon scattering in nanoscale systems: Lowest order expansion of the current and power expressions. *Journal of Physics: Conference Series*. 2006; p 247.
- (50) Rakhmilevitch, D.; Korytár, R.; Bagrets, A.; Evers, F.; Tal, O. Electron-vibration interaction in the presence of a switchable kondo resonance realized in a molecular junction. *Phys. Rev. Lett.* **2014**, *113*, 236603.

# Resolving Ambiguity of the Kondo Temperature Determination in Mechanically Tunable Single-Molecule Kondo Systems - Supplementary Information

Martin Žonda,<sup>\*,†,‡</sup> Oleksandr Stetsovych,<sup>¶</sup> Richard Korytár,<sup>†</sup> Markus Ternes,<sup>§,||</sup>  
Ruslan Temirov,<sup>||,⊥</sup> Andrea Raccanelli,<sup>#</sup> Frank Stefan Tautz,<sup>||</sup> Pavel Jelínek,<sup>¶,@</sup>  
Tomáš Novotný,<sup>†</sup> and Martin Švec<sup>\*,¶,@</sup>

<sup>†</sup>*Department of Condensed Matter Physics, Faculty of Mathematics and Physics, Charles University, Ke Karlovu 5, CZ-121 16 Praha 2, Czech Republic*

<sup>‡</sup>*Institute of Physics, Albert Ludwig University of Freiburg, Hermann-Herder-Strasse 3, 79104 Freiburg, Germany*

<sup>¶</sup>*Institute of Physics, Czech Academy of Sciences, Cukrovarnická 10, CZ-162 00 Praha 6, Czech Republic*

<sup>§</sup>*Institute of Physics II B, RWTH Aachen University, 52074 Aachen, Germany*

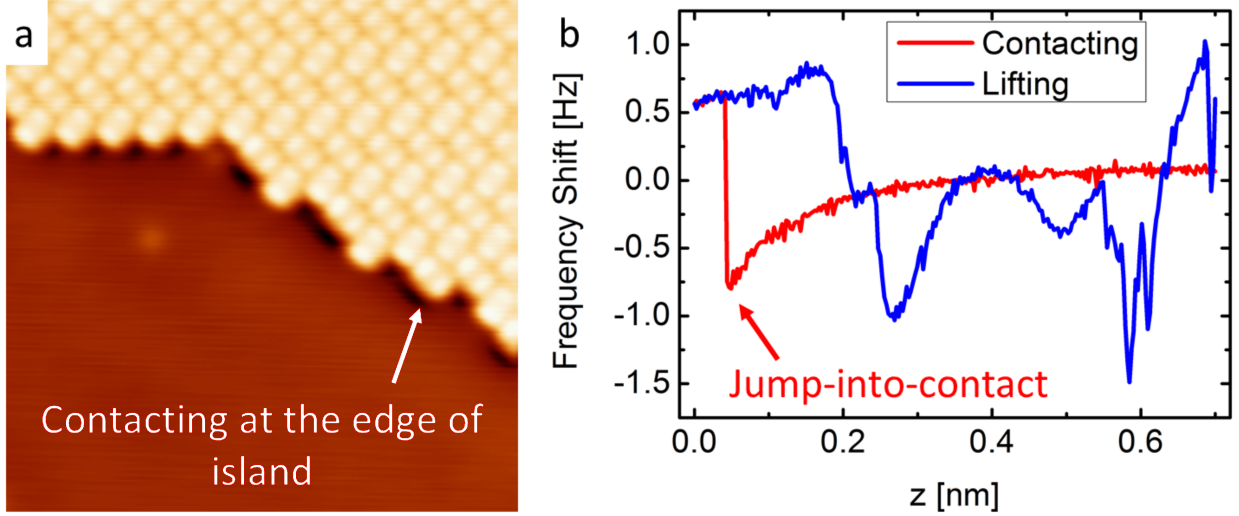
<sup>||</sup>*Peter Grünberg Institut (PGI-3), Forschungszentrum Jülich, Germany*

<sup>⊥</sup>*University of Cologne, Faculty of Mathematics and Natural Sciences, Institute of Physics II, Germany*

<sup>#</sup>*Peter Grünberg Institute (Cryo-Lab), Forschungszentrum Jülich, Germany*

<sup>@</sup>*RCPTM, Palacky University, Šlechtitelu 27, 783 71, Olomouc, Czech Republic*

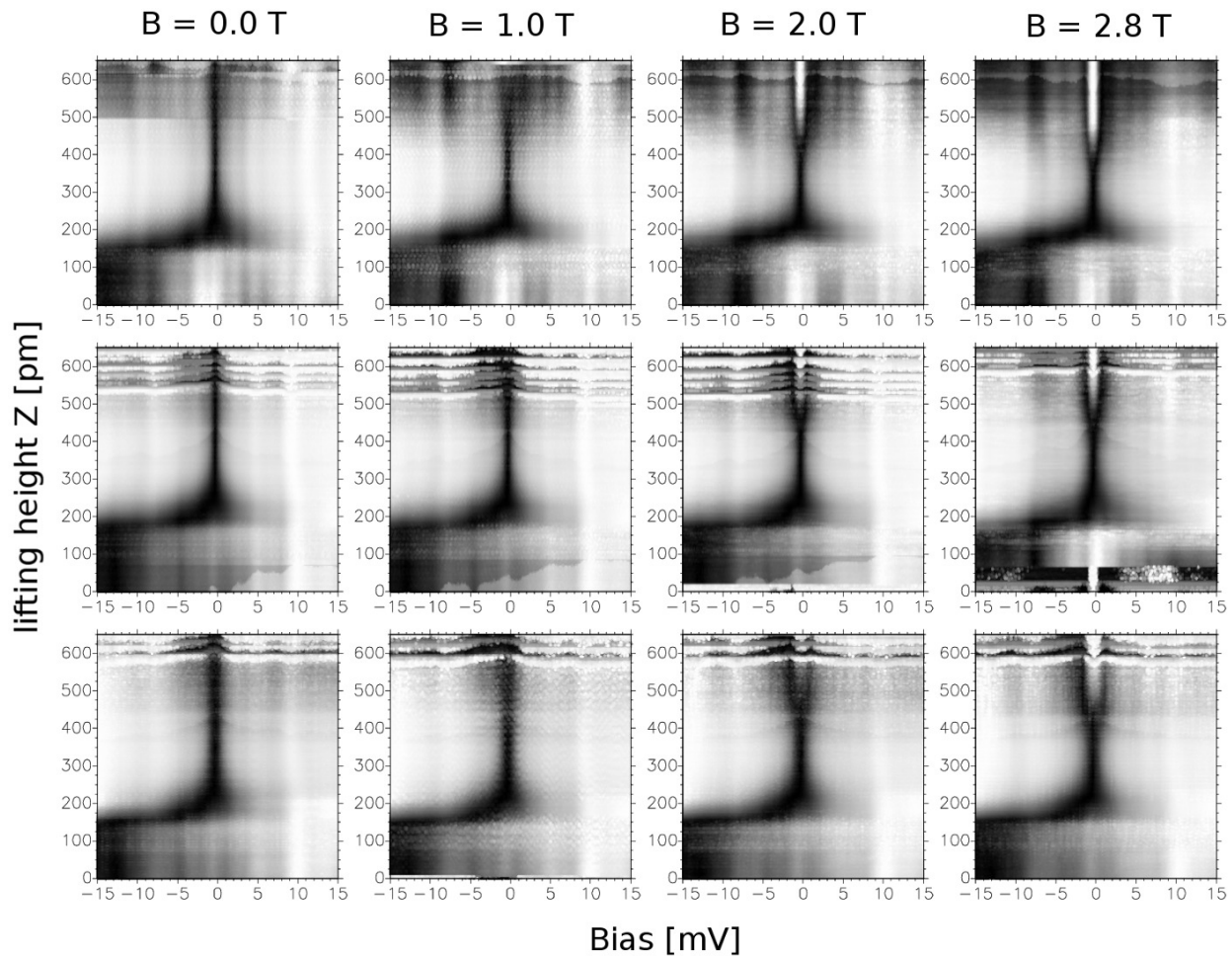
E-mail: martin.zonda@karlov.mff.cuni.cz; svec@fzu.cz



Supplementary Figure S1: The process of picking up a PTCDA molecule from the surface of Ag(111). a) STM topography image of a PTCDA island ( $V = -350$  mV,  $I = 50$  pA), with a molecule at the island boundary (marked by arrow), selected for the measurements. b) The frequency shift signal during the molecule lifting procedure, showing a jump-to contact event upon the tip approach (red) and the complex signal as a result of the PTCDA being lifted from the surface (blue).

## I Sample preparation

PTCDA (4,9,10-perylenetetracarboxylic-dianhydride) molecules of 98% purity were evaporated in ultrahigh vacuum (UHV,  $3 \times 10^{-10}$  mbar) from a Ta crucible at 670 K onto an atomically clean Ag(111) single-crystal surface kept at room temperature. Experiments were performed in UHV at a base temperature of 1.2 K using a combined atomic force and scanning tunneling microscope (AFM/STM) equipped with a He<sup>4</sup>-Joule-Thomson cooling stage (SPECS Surface Nano Analysis). The probing tip of the AFM/STM was treated before the experiment by repeatable interactions with clean Ag(111) surface until a stable metallic termination was reached. The contacting experiments were performed on PTCDA molecules on the edge of a molecular island, to minimize the chances of picking up the molecule after retraction of the tip (Fig. S1a). Each of the investigated PTCDA molecules was contacted by approaching the O site of the molecule with the probing tip until a jump-into-contact event was detected in the frequency shift channel (Fig. S1b). Once the contact was formed,  $dI/dV(V, z)$  maps were recorded by changing consecutively sample bias  $V$  and the lift distance  $z$  without breaking the contact to the molecule. We note that  $z = 400$  pm corresponds to the tip-sample distance over the PTCDA O-site at  $I = 100$  pA,  $V = -350$  mV stabilization setpoint. The  $dI/dV(V, z)$  maps were recorded on the same molecule at different magnetic fields ( $B = 0, 1, 2, 2.8$  T), see Fig. S2. During magnetic field changes the tip-PTCDA contact was loosed. Subsequently, we checked the surface area by rescanning before we recontacted the PTCDA molecule to insure that the molecule remained at the same position on the surface and that the tip structure did not change.



Supplementary Figure S2: Complete sets of the  $dI/dV$  measurements taken with three different PTCDA molecules, at four levels of magnetic field. The intensities were normalized for each lifting distance separately. The digitization noise notable in the large lifting distance is an effect due to the normalization and the limited dynamic range of the used lock-in amplifier.



## II Model and fitting procedure

We use a single-impurity Anderson model whose Hamiltonian reads

$$H = H_I + \sum_{\alpha=S,T} (H_{\alpha}^b + H_{\alpha}^h). \quad (\text{S1})$$

Here, the first term describes the interacting lowest unoccupied molecular orbital (LUMO) of the PTCDA molecule,

$$H_I = \sum_{\sigma} \epsilon_d n_{d\sigma} + U n_{d\uparrow} n_{d\downarrow} + g\mu_B B S_z, \quad (\text{S2})$$

where  $d_{\sigma}^{\dagger}$  ( $d_{\sigma}$ ) creates (annihilates) an electron with spin  $\sigma$  in the LUMO at the energy  $\epsilon_d$  and  $n_{d\sigma} \equiv d_{\sigma}^{\dagger} d_{\sigma}$ ,  $S_z \equiv (n_{d\uparrow} - n_{d\downarrow})/2$ .  $U$  represents the on-site repulsive Coulomb interaction between the electrons of opposite spin and the last term of Eq. (S2) accounts for the Zeeman energy due to an external magnetic field  $B$ .

The second term of Eq. (S1) describes the conduction bands of the substrate ( $S$ ) and the tip ( $T$ ) electrodes,

$$H_{\alpha}^b = \sum_{k,\sigma} \epsilon_{\alpha k} c_{\alpha k \sigma}^{\dagger} c_{\alpha k \sigma},$$

where  $c_{\alpha k \sigma}^{\dagger}$  ( $c_{\alpha k \sigma}$ ) creates (annihilates) an electron with spin  $\sigma$  in the state with momentum  $k$  and the energy  $\epsilon_{\alpha k \sigma}$ . Finally, the last term in Eq. (S1) accounts for the hybridization between the conduction bands and the molecular orbital enabling electrical transport through the molecule

$$H_{\alpha}^h = \sum_{k,\sigma} \left( V_{\alpha k} d_{\sigma}^{\dagger} c_{\alpha k \sigma} + h.c. \right).$$

In our numerical calculations we assume energy-independent hybridization functions  $\Gamma_{\alpha}(\epsilon) \equiv \pi \sum_k |V_{\alpha k}|^2 \delta(\epsilon - \epsilon_{\alpha k}) = \Gamma_{\alpha}$  and  $\Gamma = \Gamma_S + \Gamma_T$  is the total hybridization.

The measured  $dI/dV$  curves have been fitted using the formula for differential conductance in the tunneling regime<sup>1,2</sup>

$$\frac{dI}{dV}(V) = G \int_{-\infty}^{\infty} d\omega \pi \Gamma \rho_{\text{NRG}}(\omega, \Gamma, T, B) (-f'(\omega - eV, T)), \quad (\text{S3})$$

where the temperature- and magnetic-field-dependent spectral function  $\rho_{\text{NRG}}(\omega, \Gamma, T, B)$  calculated with numerical renormalization group theory (NRG) is convolved with the derivative of the Fermi-Dirac distribution to account for the broadening during the tunneling process. We used a band cut-off of  $\pm 10$  eV in the NRG calculations and assumed constant density of states. The NRG calculations have been performed with the open-source code NRG LJUBLJANA<sup>3,4</sup>. The finite-temperature-dependent spectral functions have been calculated using the full density matrix algorithm based on the complete Fock-space concept.<sup>4,5</sup> We have set the logarithmic discretization parameter  $\Lambda = 2$  and used the interleaved method<sup>6,7</sup> (with  $4 \leq N_z \leq 10$ ) together with Gaussian (at low frequencies) and log-Gaussian (at high-frequencies) broadenings to smooth the spectral functions. By varying both  $N_z$  and the

broadening we verified that the used values are not affecting the fits. For more detailed explanation of the NRG Ljubljana settings see its reference manual.<sup>4</sup>

Here we shortly discuss the approximations introduced to make the comparison between the experiment and model possible:

(i) We consider only a constant hybridization function. It has been shown in a recent study of a similar system (Au-PTCDA complex)<sup>2</sup> that the replacement of the function  $\Gamma(\omega)$  by its value at the Fermi energy may lead to a factor 1.5 difference in  $T_K$ . However, considering that in our study  $T_K$  changes by more than nine orders of magnitude, such a correction would not alter our conclusions.

(ii) We have truncated the parametric space by fixing the values of all parameters except  $\Gamma$  and  $G$ . As revealed by an ab-initio study of the tip/PTCDA/Ag junction<sup>8</sup> the  $U$  can vary with increasing  $z$ . We have made a complete analysis for  $U = 0.5$  eV and  $U = 1$  eV, which represent a relevant range of values extrapolated from the cited study. Because  $U$  does not significantly affect the results (see Fig. S3a), we present in the main text only the results for  $U = 1$  eV.

(iii) Because the experimentally measured Kondo resonances are nearly symmetric with respect to the Fermi level, we have assumed electron-hole symmetry and fixed the “half-filling” condition  $\epsilon_d = -U/2$ . This allows us to approximate the Kondo temperature by<sup>9,10</sup>

$$T_K = 0.29\sqrt{\Gamma U} \exp\left(-\frac{\pi U}{8\Gamma}\right). \quad (\text{S4})$$

A small systematical offset of the peak position with respect to zero bias has been accounted for by shifting the data by a constant energy of  $-0.26$  meV.

(iv) We have used the gyromagnetic factor  $g = 2$  for the free electronic spin. We have tested this value using a perturbative fitting procedure introduced by one of the coauthors<sup>11</sup>. Note that the true  $g$ -factor can slightly differ from this value because of the exchange interaction with the conduction electrons polarized by the magnetic field<sup>12</sup>.

(v) Finally, we note that the best temperature to describe the spectra of the PTCDA molecule either with Eq. (S3) or with the perturbative scattering model of Ref.<sup>11</sup> is  $T_{\text{exp}} = 1.4$  K slightly above the base temperature of 1.2 K of the experimental setup.

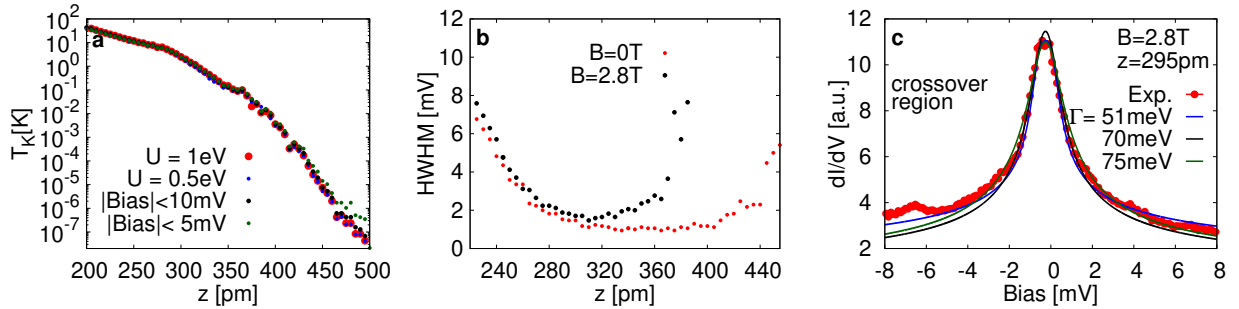
Taking into the account all above approximations we are left just with two free parameters, namely  $\Gamma/U$  and  $G$ . Still, a direct application of the fitting procedure would require an NRG calculation of the spectral function at each instance of the optimization process. A much more efficient procedure is to calculate a large set of spectral functions for a very dense mesh of  $\Gamma/U$  values (with  $\Delta\Gamma/U = 0.0001$ ) in advance. The fitting algorithm goes through this dense set, fits  $G$  and calculates the mean-square residual for each value of  $\Gamma/U$ . Because differential conductance Eq. S3 is linear in  $G$  its optimal value for any  $\Gamma/U$  can be calculated as  $G_o = C^T X / (C^T C)$ , where  $X$  is the column vector of experimental data and  $C$  is the column vector of theoretical differential conductance calculated at the experimental voltage-bias points for  $G = 1$ . The value of  $\Gamma/U$  with the minimal squared residuals is then picked as the best fit. The main reason why this is much more efficient then the direct fitting is that one can calculate each spectral functions independently which allows to use massive parallelization.

In the NRG based fits presented in the main text we have used the whole range of

the experimental voltage bias ( $[-15, 15]$  mV). However, as shown in Fig. S3a limiting the bias range to  $[-10, 10]$  mV (black circles) or even  $[-5, 5]$  mV (green circles) does not have a significant effect on the fitted  $T_K$ . We can therefore conclude that the fitting procedure is not oversensitive to the details of the tails and is primarily lead by the properties of the zero-bias anomaly as expected for the Kondo problem.

### III Fitting in the crossover region

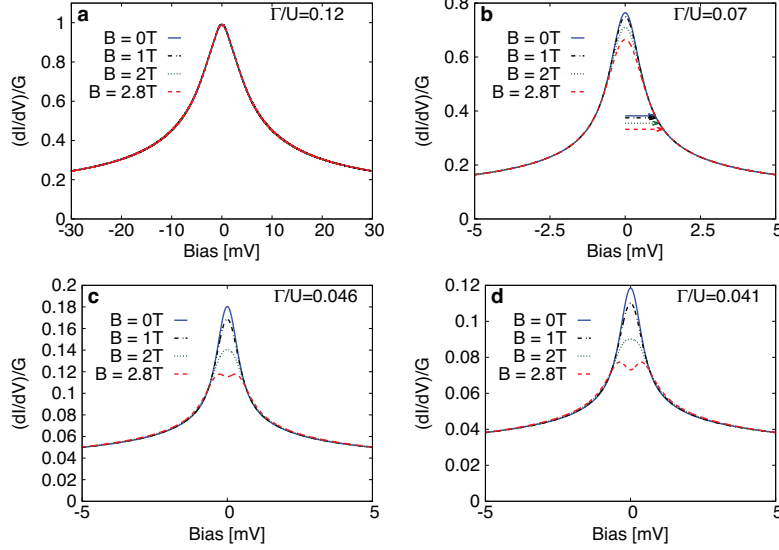
The width of the zero-bias conductance peak is in the crossover regime, where  $T_K \sim T_{\text{exp}}$ , not very sensitive to  $T_K$ . Therefore, we have found that the half-width at half-maximum (HWHM) obtained from the experimental data shows a broad, plateau-like minimum and even increases for sufficiently large  $z$  (Fig. S3b). This non-monotonous behavior is an indirect consequence of the decreasing ratio of  $T_K/T_{\text{exp}}$  which leads to decreasing intensity of the zero bias Kondo peak. Whereas for  $T_K \gg T_{\text{exp}}$  the HWHM is directly proportional to  $T_K$ , the width of the observed Kondo peak at  $T_K \lesssim T_{\text{exp}}$  is primarily defined by  $T_{\text{exp}}$ . Even worse, because the Kondo peak intensity rapidly decreases with further reduction of  $T_K$  and the shape of the peak develops to a temperature broadened logarithm<sup>11,13</sup>, the HWHM measured at a fixed energy range around zero apparently *increases*. This counterintuitive behavior is displayed in Fig. S3b and is also visible in the Frota fits shown in Fig. 2(a,b) of the main text.



Supplementary Figure S3: a) Comparison of  $T_K$  fitted with  $U = 0.5$  eV (blue) and  $U = 1$  eV (red) using the whole experimental voltage bias  $[-15, 15]$  mV and  $T_K$  fitted with  $U = 1$  eV using limited voltage bias  $[-10, 10]$  mV (black) and  $[-5, 5]$  mV (green). b) HWHM obtained directly from the experimental data for  $B = 0$  and 2.8 T. The magnetic field leads to a splitting of the conductance peak at  $z \approx 400$  pm. Therefore, the HWHM is not well defined for  $B = 2.8$  T at  $z \gtrsim 400$  pm. c) The experimental  $dI/dV$  from the crossover region fitted with different  $\Gamma$ 's. The example  $z = 295$  pm is close to the apparent step in the inset of Fig. 4a in the main text.

To overcome this problem of determining  $T_K$ , we apply an external magnetic field  $B$  strong enough to split the Kondo peak in the weak-coupling regime, that means the Zeeman energy has to be sufficiently larger than the thermal energy,  $g\mu_B B \gtrsim 2k_B T_{\text{exp}}$ . In such a  $B$ -field we can distinguish two clear limits (see Fig. S4):

(i) Kondo system in which the peak shows no splitting *and* in which the HWHM is sufficiently larger than  $k_B T_{\text{exp}}$  can be safely assumed to be in the strong-coupling regime



Supplementary Figure S4: NRG-based  $dI/dV$  simulations at different  $\Gamma/U$  ratios and magnetic fields  $B$ . a) At  $\Gamma/U = 0.12$  the system remains even at  $B = 2.8$  T in the strong coupling regime with  $k_B T_K \gg g\mu_B B$  and the spectra at different  $B$  are indistinguishable. b) In the crossover regime ( $\Gamma/U = 0.07$ ) with  $2k_B T_K \approx g\mu_B B$  only the central peak intensity is reduced. Note, that the HWHM, signalled by arrows, effectively increases with  $B$ . c)+d) In the weak coupling limit ( $\Gamma/U \leq 0.046$ ) with  $k_B T_K \ll g\mu_B B$  the split can be observed as soon as  $2k_B T_{\text{exp}} \lesssim g\mu_B B$ .

where  $T_K$  is determined by the HWHM of the peak (Fig. S4a).

(ii) Observed split peak indicates the Kondo effect in the weak-coupling regime with  $2k_B T_K \lesssim g\mu_B B$ . In this regime the HWHM is not a good indicator for  $T_K$  and, therefore, HWHM can not be used for its direct estimation from experimental data. However, because it contains two peaks one can use NRG-based or perturbative models to fit the true  $T_K$  (Fig. S4c-d).

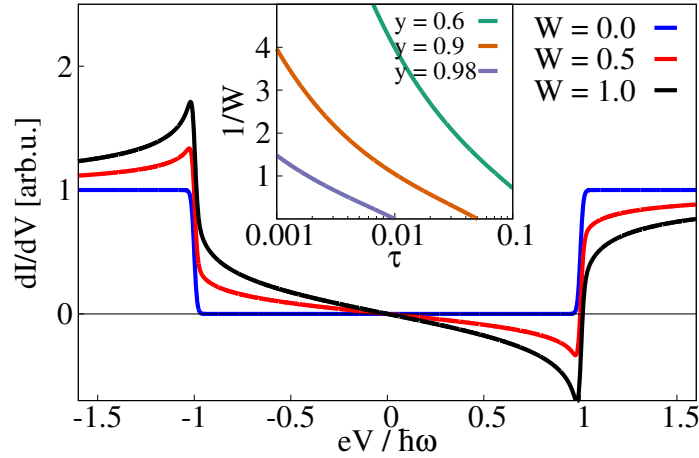
However, in the crossover regime, where the HWHM is not a good quantity for  $T_K$  because  $T_K \sim T_{\text{exp}}$ , often also the experimentally available external field is only  $k_B T_K \sim g\mu_B B$ , and therefore not strong enough to visibly split the peak. In this situation, neither of the two cases above is applicable. This is demonstrated in Fig. S3c where we plot data measured at  $z = 295$  pm and at  $B = 2.8$  T. The Kondo peak is not split, however, the HWHM is  $\approx 1.6$  mV, only a factor 4 above the minimal experimental broadening of  $3.5k_B T_{\text{exp}}/e = 0.42$  mV. Therefore, we can fit the data with a large variance in  $\Gamma$  — all three displayed curves fit the experimental data equally well (the difference in mean-square residuals between the worst and best fit is within 1%), even though their coupling to the substrate ranges from  $\Gamma = 51$  meV to  $75$  meV (taking  $U = 1$  eV) leading via Eq. (S4) to an order of magnitude difference in  $T_K$  and to the apparent step in the “direct-fit” curve shown in the inset of Fig. 4a of the main text.

Although the HWHM is not very sensitive to the change of  $T_K$  in the crossover region, the amplitude of the peak depends strongly on the external field  $B$  (see Fig. S4b and c and Fig. 4c of the main text). This enables us to compare the ratio of  $dI/dV(V = 0 \text{ mV})$

measured in two sufficiently different magnetic fields with theory calculations to determine the correct  $\Gamma$ . As explained in the main text, it is crucial to use the ratio as we need data independent of the total amplitude parameter  $G$  in Eq. (S3). The black curve in Fig. S3c shows the best fit using the above method.

The success of the fitting procedure might be surprising at the first glance, given the simplistic nature of the SIAM, containing only a single orbital. We comment on the role of other molecular orbitals and vibrational degrees in the theoretical description. As elaborated in Ref.<sup>8</sup>, the partially occupied LUMO is separated from other orbitals by at least one electronvolt. Therefore, for the low-bias window, their omission is justified. A detailed comparison of the theoretical and experimental data in Fig.2(a) in the main text reveals pairs of small side-peaks. These peaks are due to inelastic excitations of molecular vibrations.<sup>14,15</sup> Vibrational degrees of freedom are not included in our SIAM description. However, the small height of these peaks, at the threshold of the experimental resolution, implies that the respective electron vibrational coupling matrix elements are very weak. Consequently, their impact on the Kondo temperature is negligible<sup>16</sup>. We discuss these excitations in detail in the next section.

## IV Voltage – asymmetric vibrational signal



Supplementary Figure S5: Inelastic contribution to the differential conductance calculated from Ref.<sup>17</sup> for different relative weights of the anti-symmetric part  $W \equiv W^{(A)}/W^{(S)}$ . The unit of energy  $\hbar\omega$  is the energy of the vibrational excitation. The broadening is solely due to the temperature, which we set to  $k_B T = \hbar\omega/50$ . *Inset:* Dependence of  $1/W$  on electronic parameters: the elastic Landauer transmission  $\tau$  and the coupling imbalance  $y \equiv |\Gamma_T - \Gamma_S|/(\Gamma_T + \Gamma_S)$ .

The experimental  $dI/dV$  (Figs. 2 and 3 in the main text) reveal, additionally to the central resonance, peaks and dips at finite bias which we attribute to excitations of vibrational modes in the molecular junction. We observe peaks at roughly  $-7$  meV and shallow dips



around +7 meV which do not change with increasing magnetic field and only weakly respond to stretching, mainly by a non-monotonous shift of the excitation energy, similar to Ref.<sup>15</sup>.

The asymmetry of the vibrational pairs in the inelastic electron tunneling spectroscopy (IETS) was considered theoretically by Paulsson *et al.* within the self-consistent Born approximation and the lowest-order expansion<sup>14,17</sup>. Their methodology has been applied in the analysis of asymmetries in the IETS by Xu *et al.*<sup>18</sup>. To proceed with the analysis of Paulsson *et al.*<sup>14,17</sup>, we employ a simple model of the molecule which contains a single (frontier) orbital that is coupled to a single vibrational mode and a pair of leads. The resulting  $dI/dV$  can be decomposed as

$$\begin{aligned} \frac{dI}{dV}(V) = & \frac{2e^2}{h}\tau \\ & + W^{(S)}G^{(S)}(eV, \hbar\omega, k_B T) + W^{(A)}G^{(A)}(eV, \hbar\omega, k_B T), \end{aligned} \quad (S5)$$

where the first part is the elastic Landauer term ( $\tau$  being the transmission) and the remaining two terms are due to inelastic processes involving the vibration. The functions  $G^{(S/A)}$  are symmetric and anti-symmetric in voltage and are universal in the sense that they do not depend on microscopic parameters other than the vibrational frequency  $\omega$  and the temperature  $T$ . The symmetric and anti-symmetric lineshapes combine with weights  $W^{(S/A)}$ . We plot the inelastic part in Fig. S5 for different ratios  $W^{(A)}/W^{(S)} = W$ . The ratio  $W$  depends only on electronic parameters, namely, the (orbital) line-widths  $\Gamma_T$  and  $\Gamma_S$  due to the tip and the substrate, respectively, and the orbital (on-site) energy  $\epsilon_d$ . In the inset of Fig. S5 we plot  $1/W$  expressed as a function of the coupling imbalance  $y \equiv |\Gamma_T - \Gamma_S|/(\Gamma_T + \Gamma_S)$  and the elastic Landauer transmission  $\tau$ . The model predicts that the anti-symmetric signal gets more prominent (large  $W$ ) when the coupling imbalance  $y$  is large and  $\tau$  is low.

This prediction can be compared with the experimental  $dI/dV$  (Fig. 2, main text). The asymmetry of the inelastic signal is clearly visible when  $z \lesssim 350$  nm. The elastic transmission can be estimated from the  $dI/dV$  in units of  $G_0$  at  $\pm 15$  mV, where we get  $\tau \gtrsim 10^{-2}$ . Additionally, the imbalance  $y$  can be readily obtained from the fitted values of  $\Gamma_T$  and  $\Gamma_S$  displayed in Fig. 5 of the main text. For  $z \lesssim 350$  nm  $y$  approaches 0.9. According to the inset of Fig. S5, these estimates of  $\tau$  and  $y$  imply that  $W^{(A)} \approx W^{(S)}$ , which is in agreement with the observed asymmetry of the inelastic signal.

However, we emphasize that the comparison can only be made on a qualitative level, because the model by Paulsson *et al.*<sup>14,17</sup> does not apply to the Coulomb blockade, i. e. to an open shell molecule. The treatment of vibrational coupling in the Coulomb blockade with a fully developed Kondo resonance presents an open theoretical problem.

## References

- (1) Schiller, A.; Hershfield, S. Theory of scanning tunneling spectroscopy of a magnetic adatom on a metallic surface. *Phys. Rev. B* **2000**, *61*, 9036–9046.
- (2) Esat, T.; Deilmann, T.; Lechtenberg, B.; Wagner, C.; Krüger, P.; Temirov, R.; Anders, F. B.; Rohlfing, M.; Tautz, F. S. Transferring spin into an extended  $\pi$  orbital of a large molecule. *Phys. Rev. B* **2015**, *91*, 144415.

- (3) Žitko, R.; Pruschke, T. Energy resolution and discretization artifacts in the numerical renormalization group. *Phys. Rev. B* **2009**, *79*, 085106.
- (4) Žitko, R. <http://nrgljubljana.ijs.si>.
- (5) Weichselbaum, A.; von Delft, J. Sum-Rule Conserving Spectral Functions from the Numerical Renormalization Group. *Phys. Rev. Lett.* **2007**, *99*, 076402.
- (6) Campo, V. L.; Oliveira, L. N. Alternative discretization in the numerical renormalization-group method. *Phys. Rev. B* **2005**, *72*, 104432.
- (7) Žitko, R. Adaptive logarithmic discretization for numerical renormalization group methods. *Comp. Phys. Comm.* **2009**, *180*, 1271 – 1276.
- (8) Greuling, A.; Rohlfing, M.; Temirov, R.; Tautz, F. S.; Anders, F. B. Ab initio study of a mechanically gated molecule: From weak to strong correlation. *Phys. Rev. B* **2011**, *84*, 125413.
- (9) Haldane, F. D. M. Theory of the atomic limit of the Anderson model. I. Perturbation expansions re-examined. *Journal of Physics C: Solid State Physics* **1978**, *11*, 5015.
- (10) Krishna-murthy, H. R.; Wilkins, J. W.; Wilson, K. G. Renormalization-group approach to the Anderson model of dilute magnetic alloys. I. Static properties for the symmetric case. *Phys. Rev. B* **1980**, *21*, 1003–1043.
- (11) Ternes, M. Spin excitations and correlations in scanning tunneling spectroscopy. *New J. Phys.* **2015**, *17*, 063016.
- (12) Wolf, E. L.; Losee, D. L.  $g$ -shifts in the "s-d" exchange theory of zero-bias tunneling anomalies. *Phys. Lett. A* **1969**, *29*, 334.
- (13) Zhang, Y.; Kahle, S.; Herden, T.; Stroh, C.; Mayor, M.; Schlickum, U.; Ternes, M.; Wahl, P.; Kern, K. Temperature and magnetic field dependence of a Kondo system in the weak coupling regime. *Nature Comm.* **2013**, *4*, 2110.
- (14) Paulsson, M.; Frederiksen, T.; Brandbyge, M. Modeling inelastic phonon scattering in atomic-and molecular-wire junctions. *Phys. Rev. B* **2005**, *72*, 201101.
- (15) Rakhmilevitch, D.; Korytár, R.; Bagrets, A.; Evers, F.; Tal, O. Electron-vibration interaction in the presence of a switchable kondo resonance realized in a molecular junction. *Phys. Rev. Lett.* **2014**, *113*, 236603.
- (16) Roura-Bas, P.; Tosi, L.; Aligia, A. A. Nonequilibrium transport through magnetic vibrating molecules. *Phys. Rev. B* **2013**, *87*, 195136.
- (17) Paulsson, M.; Frederiksen, T.; Brandbyge, M. Phonon scattering in nanoscale systems: Lowest order expansion of the current and power expressions. *Journal of Physics: Conference Series*. 2006; p 247.

- (18) Xu, C.; Chiang, C.-l.; Han, Z.; Ho, W. Nature of Asymmetry in the Vibrational Line Shape of Single-Molecule Inelastic Electron Tunneling Spectroscopy with the STM. *Phys. Rev. Lett.* **2016**, *116*, 166101.